Lithium-Ion Batteries

DOI: 10.1002/anie.201403935

Spatiotemporal Changes of the Solid Electrolyte Interphase in Lithium-Ion Batteries Detected by Scanning Electrochemical Microscopy**

*Heinz Bülter, Fabian Peters, Julian Schwenzel, and Gunther Wittstock**

Abstract: *The solid electrolyte interphase (SEI) in lithium-ion batteries separates the highly reductive lithiated graphite from reducible electrolyte components. It is critical for the performance, durability, and safe operation of batteries. In situ imaging of the SEI is demonstrated using the feedback mode of scanning electrochemical microscopy (SECM) with 2,5-di-tert-butyl-1,4-dimethoxy benzene as mediator. The formation of the SEI is indicated by a decrease of the mediator regeneration rate. Prolonged imaging of the same region revealed fluctuation of the passivating properties on time scales between 2 min and 20 h with an inhomogeneous distribution over the sample. The implications of the approach for in situ assessment of local SEI properties on graphite electrodes are discussed with respect to studying the influence of mechanical stress on SEI reliability and the mode of action of electrolyte additives aiming at improving SEI properties.*

Lithium-ion batteries (LIB) are the main energy-storage devices for portable electronics because of the high practical energy density of approximately 150 $Wh\,kg^{-1}$, good cyclability, and low self-discharge.[1] Those properties are provided by lithium ions moving between two insertion compounds forming the battery electrodes. LIBs are also gaining ground for power tools, electric traction of vehicles, and storage of intermittently available renewable energy.[2] The high energy density stems mainly from the use of strongly reducing lithiated graphite ($[Li^+]_x[C_6^-], x \leq 1$) as the negative-electrode material. However, even organic solvents and/or electrolyte salts decompose when brought into contact with this material. Fortunately, the decomposition products form a solid electrolyte interphase (SEI)[3] on the anode, that is, an electronically insulating layer of 2–100 nm thickness.[4] It separates the electrolyte components from the lithiated graphite thus avoiding further chemical reactions while permitting the passage of Li^+ ions during charging or discharging. It also prevents the co-intercalation of solvent molecules that would cause destructive exfoliation of graphite.[5] The SEI is mainly formed during the first charging of the battery and is associated with a charge that cannot be recovered (irreversible charge).

Since LIBs can only show their superb features by kinetic stabilization through an SEI,[6] it is not surprising that substantial efforts have been devoted to the analysis of SEI components using ex situ techniques.[7] The SEI contains inorganic salt degradation products and organic compounds from the reduction of solvents and additives.[8] Moreover, there is clear evidence by ex situ scanning electron microscopic (SEM) images for lateral heterogeneity in its composition.[9] The SEI is also thought to be dynamic, that is, SEI formation and dissolution of its components may continuously occur and might be disturbed by rinsing or introduction to ultra-high vacuum,[6] emphasizing the need for local in situ analysis, for example, by scanning force microscopy (SFM) which has been performed on highly ordered pyrolytic graphite as a model electrode.[10] These electrodes are unlikely to represent the local heterogeneity of typical composite electrodes. The passivating properties of SEI on glassy carbon (GC) model electrodes have been studied by a redox probe (ferrocene) using rotating disk electrodes.[11] Redox cycling of overcharge protection agents was monitored by means of a microelectrochemical cell with two GC electrodes fixed in space.[12] The setup is very reminiscent of scanning electrochemical microscopy (SECM) which has been used for determining local interfacial kinetics on a large variety of passivated electrodes.[13] Experience from other applications raises the expectation that understanding the interplay between local structures/compositions and local reactivity can greatly aid the optimization of advanced electrode architectures.[14] Along this line Zampardi et al.[15] monitored the irreversible formation of a SEI on TiO_2-based paste negative electrodes when poised below 0.5 V vs. Li/Li^+ using the SECM feedback (FB) mode with ferrocene as redox mediator. Further temporal and spatial changes could not be resolved.

Herein the SECM FB mode (Scheme 1) was employed to investigate the SEI on graphite composite electrodes after formation in a pouch bag cell, recovery of the graphite electrodes, and mounting into an enclosed SECM cell[16] inside a glove box (Supporting Information SI-1, SI-2). The mediator was 2,5-di-*tert*-butyl-1,4-dimethoxy benzene (DBDMB) in 1 M $LiPF_6$ in ethylene carbonate (EC):diethyl carbonate (DEC) 1:1. While DBDMB is new as a SECM

[*] M. Sc. H. Bülter, Prof. Dr. G. Wittstock
Department of Chemistry, Carl v. Ossietzky University of Oldenburg
26111 Oldenburg (Germany)
E-mail: gunther.wittstock@uni-oldenburg.de
M. Sc. F. Peters, Dr. J. Schwenzel
Fraunhofer Institute of Advanced Manufacturing Technology and Advanced Materials IFAM
Wiener Strasse 12, 28359 Bremen (Germany)

[**] We thank Ms. Dorothee Schuhmacher and Ms. Caroline Valedevino Moitinho, an undergraduate intern from the Universidade de São Paulo, Brazil, for technical assistance in conduction of long-term uninterrupted SECM experiments and Mr. Sebastian Jentzsch for contributing to the design and assembly of the pouch bag cells. The study is funded by the Lower Saxony Ministry of Science and Culture for IFAM and within the graduate program for Energy Storage and Electromobility (GEENI).

Supporting information for this article is available on the WWW under http://dx.doi.org/10.1002/anie.201403935.

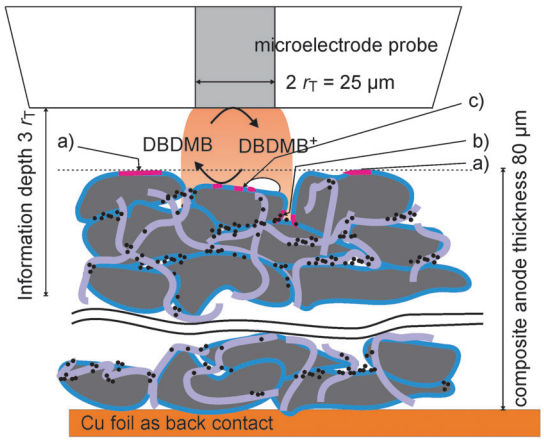

Scheme 1. SECM FB experiments at the SEI of composite electrodes made of graphite particles (gray), carbon black (black), and PVDF binder (violet). The SEI (blue) is subject to local changes (red) resulting from a) a mechanical contact by the ME, b) sliding of particles against each other, and c) spontaneous dissolution processes, gas-bubble formation, or detachment and stress within individual particles. The information depth of SECM FB experiments (ca. 3 r_T) is highlighted by a light red background.

mediator, it has been used as overcharge protection additive in LIB.[17] Its reversible oxidation to DBDMB$^+$ provides an exceptional stable diffusion-controlled steady-state current at a Pt microelectrode (ME) at a probe potential of $E_T = 4.1$ V vs. Li/Li$^+$ (SI-3) enabling experimentation over extended time spans—much longer than all our previous experiments with ferrocene derivatives.[18]

SECM approach curves to pristine and SEI-covered graphite electrodes are shown in Figure 1 as normalized current $I_T = i_T/i_{T,\infty}$ ($i_{T,\infty}$ is experimental, diffusion-limited ME current at quasi-infinite distance to the sample) versus normalized distance $L = d/r_T$ (d is the distance, r_T the radius of the ME). I_T over pristine graphite at open circuit potential (E_S(OCP) ≈ 3.36 V vs. Li/Li$^+$) is only slightly smaller than the calculated response for an infinitely fast DBDMB regeneration at the sample (Figure 1, curve 3). After lithiation the E_S(OCP) = 0.134 V vs. Li/Li$^+$ (Figure SI-4) was more negative and governed by the Li(graphite)/Li$^+$ redox couple, while at pristine graphite the DBDMB/DBDMB$^+$ mediator determines the OCP. Despite the higher driving force, DBDMB showed much smaller regeneration kinetics at lithiated graphite processed with the same amount of (insulating) binder and carbon (Figure 1, curves 2a,b). The approach curves were, however, distinguishable from pure hindered diffusion above an insulating, inert sample (Figure 1, curve 4) demonstrating that DBDMB$^+$ can traverse through the electronically insulating SEI and react with finite rate at the lithiated graphite.

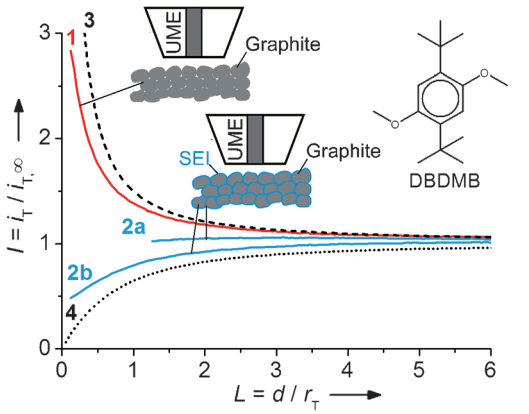

Figure 1. SECM FB approach curves to a pristine graphite electrode (1) and different charged graphite electrodes after SEI formation (2); for comparison the calculated curves for diffusion-controlled regeneration of DBDMB at the sample (3) and for an inert insulating surface (4) are shown. Further details in SI-4.

There are also significant differences between the approach curves from different regions of SEI-covered graphite electrodes (Figure 1, curves 2a vs. 2b) pointing towards lateral heterogeneity in the passivating properties of the SEI. Figure 2 shows SECM FB images of a SEI-covered

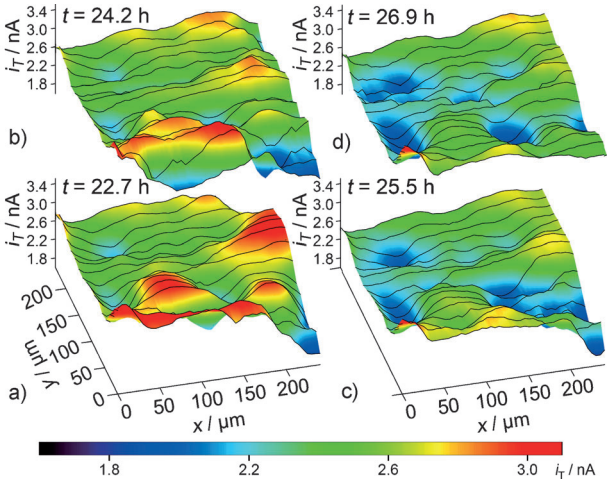

Figure 2. SECM feedback image of an identical region of a SEI-covered graphite electrode recorded a) 22.7 h, b) 24.2 h, c) 25.5 h, and d) 26.9 h after filling electrolyte solution in the SECM cell at $d \approx 3$ µm. Experimental details in SI-5.

graphite electrode. They were selected from a much longer sequence shown in Supporting Information SI-9. Similar behavior has been observed on five samples. Owing to the roughness of the graphite electrode, varying SECM currents are expected as a result of a change in working distance d (experimental roughness was $R_a = 2.5$ µm (SI-1)) and because of lateral differences in the regeneration kinetics. From an individual image, it is impossible to disentangle both influences. Alternative imaging approaches are not readily applicable as discussed in SI-6. Provided that those features do not change with time, relative $i_T(x,y)$ should remain constant within a sequence recorded above an identical region. Indeed, SEI-covered electrodes showed some regions where currents remained stable over hours, such as, in the rear parts of Figure 2 a–d. Other regions showed quite drastic changes in their response. The region around (x/µm, y/µm) = (200, 50) exhibited initially high $i_T(x,y)$ (vs. to the average ME current $\langle i_T \rangle$ of the image) in Figure 2 a, but changed to low $i_T(x,y)$ in

Figure 2c. The region around (240,0) constitutes an example for the opposite trend: A relatively small $i_T(x,y)$ in Figure 2a increased within 4 h to the values in Figure 2d. These changes cannot be explained by topographic differences alone because the sample was not touched or deformed during this time. It rather reflects the spatial and temporal heterogeneity of SEI properties.

A comparison between forward and backward line scans (Figure 3) above the same region revealed changes of SEI properties occurring within 5 min that are not obvious from a comparison of entire image frames in Figure 2. Figure 3

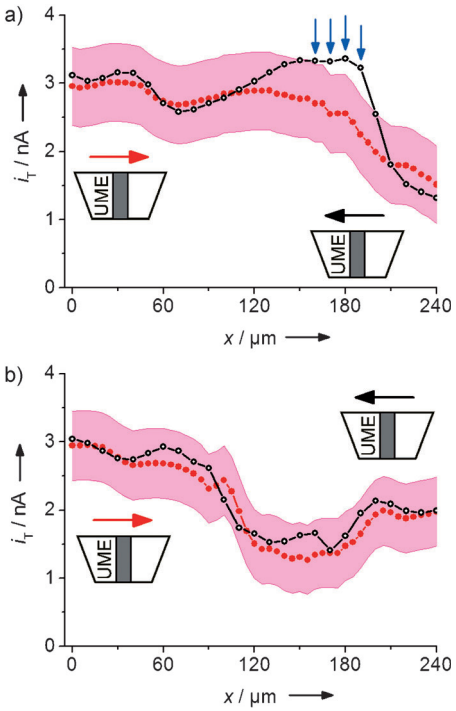

Figure 3. Comparison of forward and reverse line scans on the same region a) with short-term change and b) without a clearly detected short-term change. See text for details.

shows selected line scans of the same region extracted at different times from one image sequence (Figure SI-9). Figure 3a shows an example where forward and backward scans almost perfectly retrace except between $120 \leq x/\mu m \leq 210$. In this region a substantial difference between the corresponding forward and backward scans is clearly visible. Such features were observed mainly in regions close to a region of reduced currents (low $i_T(x,y)$) that probably represented protruding SEI-covered graphite particles. In contrast, many pairs of forward/backward line scans show only small deviations, such as in Figure 3b. Such deviations rarely exceeded 8% of $\langle i_T \rangle$ above unlithiated graphite, which is considerably lower than those deviations in Figure 3a.

To substantiate the observation that short-term current variations were concentrated in specific regions, two-dimensional color-coded histograms were constructed (Figure 4a,d) by counting the "events" that $i_T(x, y)$ at a specific grid point in the reverse line scan deviated by more than $0.21\langle i_T \rangle$ from

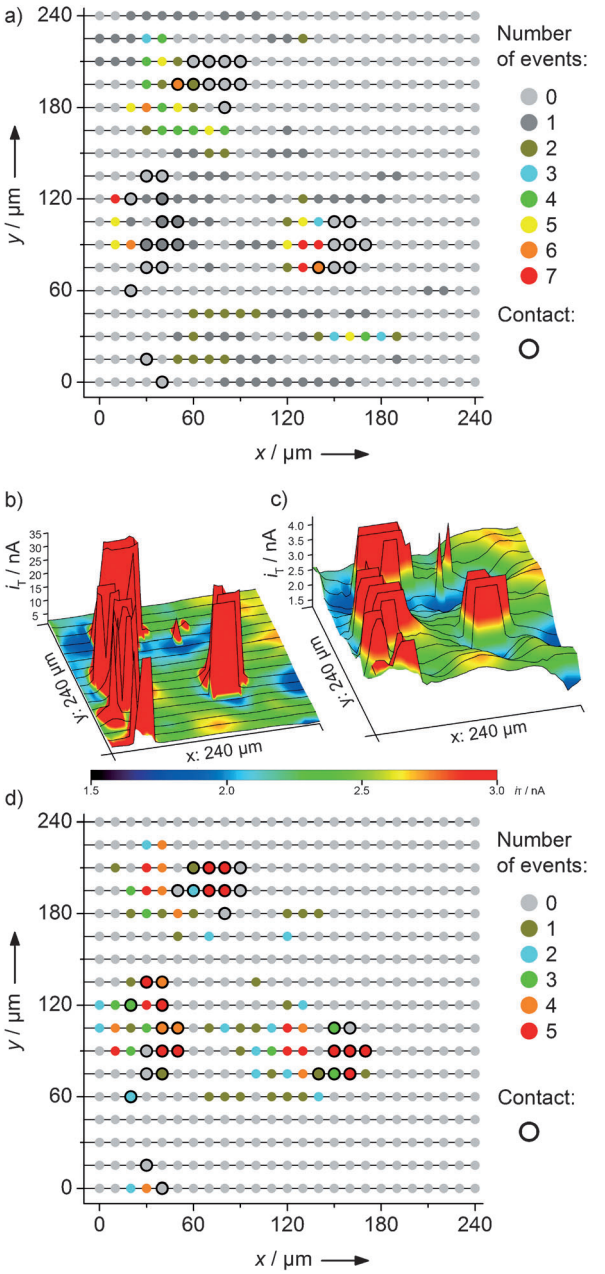

Figure 4. Local SEI instability. Color codes show the number of events with current variations of more than 0.21 $\langle i_T \rangle$ in a sequence of eight (a) and five (d) SECM FB images. FB images during contact (b, $d \approx 0$) showing overflows and at the same time (c) providing local features. Full data sets and imaging conditions are provided in SI-5.

$i_T(x, y)$ in the forward scan at the same position. The 21% margin is indicated in Figure 3 as a shaded band and was selected to prevent counting of incidental variations due to experimental imperfections. 69% of the grids points did not show a single event, whereas 13% of all grid points showed more than one event. Evaluation of further samples with this procedure yielded a rather stable fraction of points showing more than one event (6 to 21%). 28 h after filling the SECM cell and recording several images (SI-5), the ME was incrementally moved towards the graphite electrode until the ME just touched protruding sample regions (region (a) in

Scheme 1). This condition is very easily detected by short-circuit currents in Figure 4b causing an overflow of the potentiostat. In other regions, i_T still followed the trends (Figure 4c) from preceding and subsequent images of the entire sequence (SI-5). The locations of mechanical contact in Figure 4b are indicated in the histograms (Figure 4a,d) by open circles. It seemed that the mechanical contact occurred preferentially at regions that had exhibited lower signals in the preceding image sequence (c.f. Figure 2c,d). Before mechanical contact those regions would have exhibited approach curves in which i_T decreases monotonically with decreasing d (c.f. Figure 1, curve 2b). The high-current regions in Figure 4b have sizes and shapes typical for graphite particles (Figure SI-1) indicating that those particles are relatively flat. Regions with high numbers of "events" in Figure 4a are located close to, but rarely at those contact positions. Only 6% of the contact positions matched the positions with multiple events before contact! We conclude that 1) those local changes of the SEI are not caused by interaction with the ME and 2) that they are caused by SEI damage in the contact zone between particles of the upper layers (Scheme 1, regions b).

During contact, the SEI is likely to be damaged locally. After completing the acquisition in Figure 4b, the ME was retracted by 3 μm and imaging was continued (Figure SI-11). In this sequence, 61% of the contact positions showed multiple events in which $i_T(x, y)$ of forward and backward currents deviated by more than $0.21\langle i_T\rangle$ (Figure 4d). Clearly, the regeneration of the damaged SEI is accompanied by strong temporal changes of the passivating SEI properties. This is consistent with our observations after incidental contact between ME and SEI on samples that had to be abandoned.

Figure 5a shows a smooth image with currents around 6 nA with a stable topographic feature at the rear right corner used to verify identical locations within the sequence ($i_{T,\infty} = 5.8$ nA). In Figure 5b a region with i_T around 1 nA developed in the front left corner. Looking at the approach curves in Figure 1, such a dramatic decrease can only be explained if a surface with finite kinetics (c.f. Figure 1, curves 2) changes to a totally inert surface (c.f. Figure 1, curve 4) and d decreases. Changes of working distances can occur for different reasons, for example, swelling or release of mechanical stress in the calendered composite electrode. However, such drastic simultaneous changes of topography and passivating properties are in contrast to the more gradual developments in Figure 2 or short-term fluctuations of smaller amplitude in Figure 3. The sharp edge of this region is also remarkable and not typical for the features detected in Figure 2. Moreover, two new regions of similar low current develop at the left rear part of the image in Figure 5c. These features disappear in Figure 5d, that is, 1 h after recording of Figure 5c. At the same location new features with low i_T reappear in Figure 5e.

Taken together the drastic current decrease, the sharp border of the affected regions, the "sudden" appearance, disappearance and re-appearance of the feature let us tentatively assign it to the formation, detachment, and re-formation of gas bubbles at the composite electrode. Gas

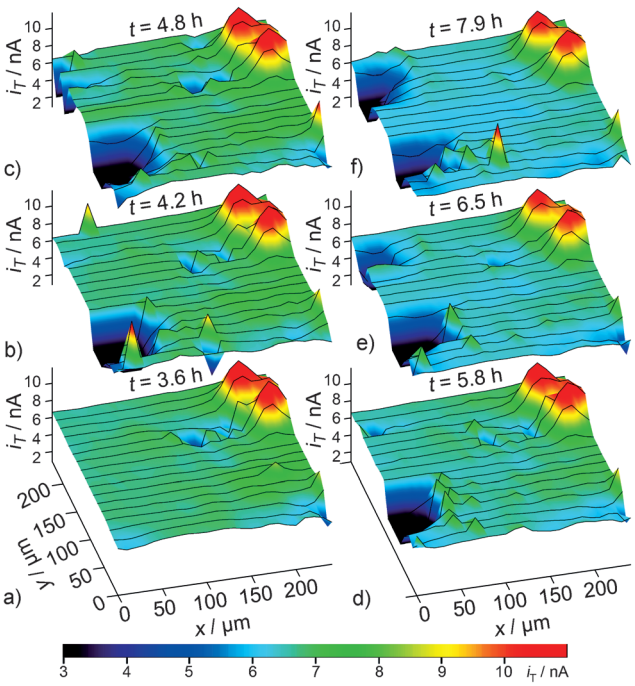

Figure 5. Detection of gas-bubble formation within a sequence of SECM FB images of an identical region of a SEI-covered graphite electrode recorded a) 3.6 h, b) 4.2 h, c) 4.8 h, d) 5.8, e) 6.5 h, and f) 7.9 h after filling electrolyte solution in the SECM cell at $d \approx 3$ μm. The complete sequence and imaging conditions are provided in SI-5.

formation at the graphite | SEI interface followed by rupture of the SEI has recently been proposed based on the detection of gaseous products and ex situ SEM images.[19] A gas bubble constitutes an electrically insulating obstacle to mediator diffusion that protrudes from the composite electrode (decrease of working distance). Thus, it could perfectly explain the strong local decrease of $i_T(x,y)$. Owing to the gas–liquid interface, the areas of low current have sharp borders. Note that the location of the features assigned to bubbles is surrounded by smaller current variations indicative for a destabilized SEI.

In conclusion, spontaneous spatiotemporal changes of SEI properties were detected in situ on a typical graphite negative electrode for the first time. Such changes show specific signatures in SECM images and might be due to volume changes during charging/discharging, dissolution of SEI components, or gas formation (Scheme 1, regions c). Gas-bubble formation and detachment have been detected in situ and differentiated from more gradual changes of SEI properties (Figure 5). The preferred occurrence of short-term events (Figure 4) close to the perimeter of what appears to be individual carbon particles may indicate mechanical disruption of the SEI inside the porous composite material (Scheme 1, regions b). It is plausible that this local SEI damage can be caused by relative small movement of particles as a result of volume expansion during lithiation, swelling of polymeric binder, and/or relaxation of mechanical stress introduced by calendering. Those spontaneous changes can be very clearly distinguished from SEI damage arising from mechanical contact with the ME body (Scheme 1, regions a).

Any damage to the SEI is detrimental to battery life time because electrolyte constituents are consumed during re-formation of the SEI. At uncovered graphite, deposition of metallic lithium may occur during charging and compromise battery safety. Therefore, it is important that incidental defects of the SEI will self-heal. Re-passivation of damaged regions was monitored in situ and takes several hours during which the regions remain susceptible to further short-term current variation. Further research using this methodology will certainly address the mode of action of solution additives on SEI formation/stability, the response of SEI during cycling and towards well defined mechanical stress as well as the existence and properties of SEI on other battery electrodes.

Received: April 3, 2014
Revised: May 29, 2014
Published online: July 30, 2014

Keywords: electrochemistry · in situ analysis · lithium-ion battery · scanning probe microscopy · solid electrolyte interphase (SEI)

[1] C. D. Rahn, C. Y. Wang, *Battery Systems Engineering*, Wiley, **2012**.
[2] B. Dunn, H. Kamath, J.-M. Tarascon, *Science* **2011**, *334*, 928.
[3] E. Peled, *J. Electrochem. Soc.* **1979**, *126*, 2047.
[4] K. Edström, M. Herstedt, D. P. Abraham, *J. Power Sources* **2006**, *153*, 380; T. Yoshida, M. Takahashi, S. Morikawa, C. Ihara, H. Katsukawa, T. Shiratsuchi, J.-i. Yamaki, *J. Electrochem. Soc.* **2006**, *153*, A576.
[5] D. Aurbach, E. Zinigrad, Y. Cohen, H. Teller, *Solid State Ionics* **2002**, *148*, 405.
[6] P. Verma, P. Maire, P. Novák, *Electrochim. Acta* **2010**, *55*, 6332.
[7] P. Niehoff, S. Passerini, M. Winter, *Langmuir* **2013**, *29*, 5806; A. M. Andersson, A. Henningson, H. Siegbahn, U. Jansson, K. Edström, *J. Power Sources* **2003**, *119–121*, 522; E. Peled, D. Bar Tow, A. Merson, A. Gladkich, L. Burstein, D. Golodnitsky, *J. Power Sources* **2001**, *97–98*, 52; M. Dollé, S. Grugeon, B. Beaudoin, L. Dupont, J. M. Tarascon, *J. Power Sources* **2001**, *97–98*, 104; M. E. Spahr, T. Palladino, H. Wilhelm, A. Wuersig, D. Goers, H. Buqa, M. Holzapfel, P. Novák, *J. Electrochem. Soc.* **2004**, *151*, A1383.
[8] V. Etacheri, R. Marom, R. Elazari, G. Salitra, D. Aurbach, *Energy Environ. Sci.* **2011**, *4*, 3243.
[9] E. Peled, D. Golodnitsky, G. Ardel, *J. Electrochem. Soc.* **1997**, *144*, L208; W. Märkle, C.-Y. Lu, P. Novák, *J. Electrochem. Soc.* **2011**, *158*, A1478.
[10] S.-K. Jeong, M. Inaba, Y. Iriyama, T. Abe, Z. Ogumi, *J. Power Sources* **2003**, *119–121*, 555; A. v. Cresce, S. M. Russell, D. R. Baker, K. J. Gaskell, K. Xu, *Nano Lett.* **2014**, *14*, 1405; Z. Jing, Z. Kaiyang in *Nanotechnology for Sustainable Energy*, *Vol. 1140*, American Chemical Society, Washington, **2013**, p. 23.
[11] M. Tang, J. Newman, *J. Electrochem. Soc.* **2011**, *158*, A530.
[12] L. M. Moshuchak, M. Bulinski, W. M. Lamanna, R. L. Wang, J. R. Dahn, *Electrochem. Commun.* **2007**, *9*, 1497.
[13] B. Liu, A. J. Bard, M. V. Mirkin, S. E. Creager, *J. Am. Chem. Soc.* **2004**, *126*, 1485; S. E. Pust, D. Scharnweber, C. Nunes Kirchner, G. Wittstock, *Adv. Mater.* **2007**, *19*, 878; Y. González-García, J. M. C. Mol, T. Muselle, I. De Graeve, G. Van Assche, G. Scheltjens, B. Van Mele, H. Terryn, *Electrochem. Commun.* **2011**, *13*, 169; F. Forouzan, A. J. Bard, M. V. Mirkin, *Isr. J. Chem.* **1997**, *37*, 155.
[14] E. Klusmann, J. W. Schultze, *Electrochim. Acta* **2003**, *48*, 3325; S. Schmachtel, S. E. Pust, K. Kontturi, O. Forsen, G. Wittstock, *J. Appl. Electrochem.* **2010**, *40*, 581; A. R. Zeradjanin, N. Menzel, W. Schuhmann, P. Strasser, *Phys. Chem. Chem. Phys.* **2014**, *16*, 13741.
[15] G. Zampardi, E. Ventosa, F. La Mantia, W. Schuhmann, *Chem. Commun.* **2013**, *49*, 9347.
[16] W. Nogala, K. Szot, M. Burchardt, F. Roelfs, J. Rogalski, M. Opallo, G. Wittstock, *Analyst* **2010**, *135*, 2051.
[17] J. Chen, C. Buhrmester, J. R. Dahn, *Electrochem. Solid-State Lett.* **2005**, *8*, A59; J. H. Chen, L. M. He, R. L. Wang, *J. Electrochem. Soc.* **2012**, *159*, A1636.
[18] G. Wittstock, H. Emons, M. Kummer, J. R. Kirchhoff, W. R. Heineman, *Fresenius J. Anal. Chem.* **1994**, *348*, 712; G. Wittstock, T. Wilhelm, S. Bahrs, P. Steinrücke, *Electroanalysis* **2001**, *13*, 669; C. Zhao, I. Zawisza, M. Nullmeier, M. Burchardt, M. Träuble, I. Witte, G. Wittstock, *Langmuir* **2008**, *24*, 7605.
[19] P. Lu, C. Li, E. W. Schneider, S. J. Harris, *J. Phys. Chem. C* **2014**, *118*, 896.

